

Traffic-Aware Multi-Camera Tracking of Vehicles Based on ReID and Camera Link Model

Hung-Min Hsu
hmhsu@uw.edu
University of Washington
Seattle, Washington

Yizhou Wang
ywang26@uw.edu
University of Washington
Seattle, Washington

Jenq-Neng Hwang
hwang@uw.edu
University of Washington
Seattle, Washington

ABSTRACT

Multi-target multi-camera tracking (MTMCT), i.e., tracking multiple targets across multiple cameras, is a crucial technique for smart city applications. In this paper, we propose an effective and reliable MTMCT framework for vehicles, which consists of a traffic-aware single camera tracking (TSCT) algorithm, a trajectory-based camera link model (CLM) for vehicle re-identification (ReID), and a hierarchical clustering algorithm to obtain the cross camera vehicle trajectories. First, the TSCT, which jointly considers vehicle appearance, geometric features, and some common traffic scenarios, is proposed to track the vehicles in each camera separately. Second, the trajectory-based CLM is adopted to facilitate the relationship between each pair of adjacently connected cameras and add spatio-temporal constraints for the subsequent vehicle ReID with temporal attention. Third, the hierarchical clustering algorithm is used to merge the vehicle trajectories among all the cameras to obtain the final MTMCT results. Our proposed MTMCT is evaluated on the CityFlow dataset and achieves a new state-of-the-art performance with IDF1 of 74.93%.

CCS CONCEPTS

• **Computing methodologies** → **Tracking; Computer vision tasks; Neural networks.**

KEYWORDS

MTMCT, multi-camera tracking, traffic-aware single camera tracking, camera link model, vehicle ReID, hierarchical clustering

ACM Reference Format:

Hung-Min Hsu, Yizhou Wang, and Jenq-Neng Hwang. 2020. Traffic-Aware Multi-Camera Tracking of Vehicles Based on ReID and Camera Link Model. In *Proceedings of the 28th ACM International Conference on Multimedia (MM '20)*, October 12–16, 2020, Seattle, WA, USA. ACM, New York, NY, USA, 9 pages. <https://doi.org/10.1145/3394171.3413863>

1 INTRODUCTION

Due to the exponential growth of the deployed surveillance cameras with networking supports, the opportunity to take advantage of the rich information from the multi-camera systems is immense.

Permission to make digital or hard copies of all or part of this work for personal or classroom use is granted without fee provided that copies are not made or distributed for profit or commercial advantage and that copies bear this notice and the full citation on the first page. Copyrights for components of this work owned by others than ACM must be honored. Abstracting with credit is permitted. To copy otherwise, or republish, to post on servers or to redistribute to lists, requires prior specific permission and/or a fee. Request permissions from permissions@acm.org.

MM '20, October 12–16, 2020, Seattle, WA, USA

© 2020 Association for Computing Machinery.

ACM ISBN 978-1-4503-7988-5/20/10...\$15.00

<https://doi.org/10.1145/3394171.3413863>

Among the techniques for multi-camera systems, multi-target multi-camera tracking (MTMCT) is important for traffic flow optimization and anomaly detection. Basically, MTMCT consists of two sub-tasks: 1) Single camera tracking (SCT): Detection and tracking of the objects within each single camera; 2) Inter-camera tracking (ICT): Associations of the object trajectories across different cameras. Overall, MTMCT is aimed to obtain the trajectories of every object in the scene through all the cameras in the system.

However, MTMCT is a very challenging task due to unreliable object detection, heavy occlusion, low resolution, and varying lighting and viewing-perspective conditions. Recently, many proposed works for MTMCT take into account target motion and human pose. Among these works, most of them are person based MTMCT, which only considers humans as the tracking targets. For vehicles, this task becomes more challenging because: 1) vehicles may stop for a long time at the traffic signs and continually be occluded among each other, which makes occlusion even more severe; 2) inter-class similarity for vehicles is higher because there may exist many different identities with the similar appearance.

To solve these two aforementioned challenges, we propose a novel MTMCT framework, which mainly consists of two innovations, i.e., traffic-aware single camera tracking (TSCT) and the trajectory-based camera link model (CLM).

First, TSCT is proposed to handle the long-term occlusions created in the traffic scenarios. Usually, there will be a large number of isolated and fragmented vehicle trajectories, created from a single camera multi-target tracker like the TrackletNet tracker (TNT) [38], in the center of the frames where vehicles do not enter or exit the camera's field of view (FoV). For example, when a vehicle stops in front of a red traffic light, it can be partially or even fully occluded in the camera's FoV for a long time. We would like to call this kind of zone as a traffic-aware zone. According to this condition, TSCT is proposed to find out the traffic-aware zones, where this kind of occlusion happens, by clustering the start and end nodes of all the resulting trajectories from the TNT. Vehicle Re-ID in the single camera is then implemented for these traffic-aware zones to connect these disconnected trajectories created in the traffic scenarios.

Second, facing higher inter-class appearance similarity of distinct vehicles, trajectory-based CLM is further proposed to impose spatio-temporal constraints and reduce solution search space for the cross camera ReID. For two different vehicles with a very similar appearance, it is nearly impossible to re-identify them using a typical ReID method. However, taking advantage of the spatial and temporal constraints between a pair of adjacently connected cameras, we can easily filter out the vehicles that are not likely to appear in a certain camera at a certain timestamp. We define

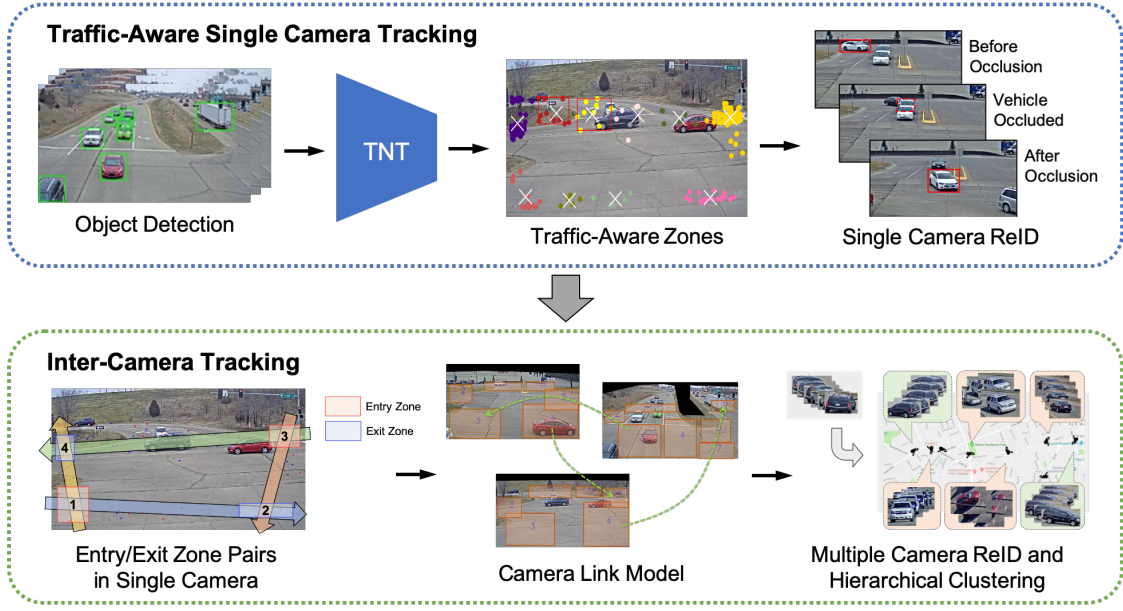


Figure 1: The illustration of our MTMCT framework. First, a single camera tracker TNT appended by our TSCT is utilized to obtain SCT results for each camera. Second, CLMs with entry/exit zones and transition times are automatically generated. Third, vehicle ReID with temporal attention is implemented on the solution space from the CLM. Finally, the hierarchical clustering is involved for the final MTMCT results.

these constraints, including the vehicle entry/exit zones and the transition times, as the CLM. Using the CLM automatically generated from the training data, vehicle ReID within the same camera becomes much more accurate and efficient.

Finally, a hierarchical clustering algorithm, based on the Euclidean distance between the feature space of different trajectories, is used to merge the trajectories among all the cameras to obtain the final MTMCT results.

Overall, the framework of our proposed MTMCT is shown in Fig. 1. First, we use the TNT [38] to obtain SCT results for each camera. Based on the results from the TNT, our proposed TSCT can generate the traffic-aware zones and perform vehicle ReID within each camera to solve the occlusion problem. We then analyze the vehicle trajectories in the training dataset and automatically generate the CLM, i.e., the entry/exit zones and the transition times, for each camera. After that, vehicle ReID with temporal attention is implemented on the solution space from the CLM. Finally, the hierarchical clustering is introduced for the final MTMCT results. To summarize, we claim the following contributions:

- Propose a new MTMCT framework specifically designed for vehicles.
- Utilize a novel TSCT strategy to improve vehicle SCT results, considering common traffic scenarios.
- Create a trajectory-based CLM generation method that adds spatio-temporal constraints and reduces the solution space for cross camera vehicle ReID.
- Achieve a new state-of-the-art performance on the CityFlow dataset.

The rest of the paper is organized as follows. In Section 2, we provide an overview of the related works. Our proposed framework for MTMCT of vehicles is introduced in Section 3. Section 4 presents our experimental results of the proposed MTMCT framework on the CityFlow dataset [36]. Finally, the conclusion is drawn in Section 5.

2 RELATED WORKS

Single camera multi-object tracking. Tracking-by-detection based multi-object tracking (MOT) approaches [5, 42] are the most popular schemes for single camera tracking. Moreover, graph model based tracking methods [2, 14, 22, 31–33, 37, 39] are another classical schemes, i.e., each detected object is represented as a vertex to form a graph with edges denoting the affinity (similarity) between two detections between two image frames, while in some works [2, 31, 37, 39], a vertex denotes a tracklet formed from some association rules, with the edges denoting the affinity between two disconnected tracklets. The appearance feature plays a vital role in the tracking-by-detection framework. Many different types of appearance features are applied to deal with SCT. For example, CNN-based features have been widely used for ReID tasks [27, 33, 44, 46], where metric learning is exploited to train the CNN-based features [27]. Furthermore, appearance features and temporal features can be combined [22, 37, 44] to achieve better performance. However, all of these methods could not deal with the long occlusion due to the traffic scenarios.

Camera link model. A camera link model (CLM) consists of camera link information and transition time distribution of a pair of adjacently connected cameras, i.e., a camera link model takes

spatio-temporal constraints into consideration. In MTMCT, a CLM can be used as effective constraints to reduce the search space of matching so as to improve the performance of MTMCT, as evidenced in some works [11, 15, 36, 37]. For example, Lee et al. [15] use the CLM to estimate bidirectional transition time distribution in an unsupervised scheme for MTMCT. Tang et al. [36, 37] and Hsu et al. [11] also use the car speed to generate the transition time distribution for each connected pair of adjacently connected cameras. Therefore, the accuracy of MTMCT can be significantly improved by CLM by reducing the candidate set of matching. In this paper, we systematically generate the CLMs to assist the ReID in the MTMCT tasks.

Appearance feature based vehicle ReID. Vehicle ReID has attracted more research efforts in the past few years. For vehicle-based ReID, VeRi-776 [17] and VeRi-Wild [20] are the most widely used benchmarks, which not only provide high quality annotations but also the camera deployment geometry. In ReID, there are two types of appearance feature extraction methods. One is traditional handcrafted methods, such as SURF [1] and ORB [28]. The other is CNN-based methods [21, 41, 45], which have been proven to achieve better performance than traditional handcrafted methods in the past years. Thus, recent methods [17, 19, 43] focus on learning an embedding model that maps the samples into an embedding space. Liu et al. [17] propose a mixed difference network using a vehicle model and ID information to construct more robust feature embedding. Liu et al. [19] propose a “PROVID” ReID model by using visual feature, license plate and spatio-temporal information for the vehicle ReID task. Shen et al. [29] incorporate complex spatio-temporal information for effectively regularizing the ReID results by a two-stage framework. Based on a multi-view inference scheme, Zhou et al. [47] generate a global-view feature representation to improve the vehicle ReID. Huang et al. [12] utilize car key points to train orientation-based embedding for vehicle ReID. Tang et al. [35] propose a pose-aware multi-task re-identification (PAMTRI) framework by explicitly reasoning about vehicle pose, shape, color, and types. In this work, we propose a trajectory-based CLM to enhance the performance of vehicle ReID.

3 PROPOSED METHOD

There are four steps in our proposed method, as illustrated in Fig. 1. First, we apply TSCT after a single camera tracker TNT, as presented in Section 3.1. Then, the camera links are established based on the generated entry/exit zones, as illustrated in Section 3.2. Moreover, we utilize a vehicle ReID method by combining the temporal attention and batch sampling for inter-camera tracking, as explained in Section 3.3. Finally, we use the hierarchical clustering to merge the tracklets into object trajectories, as described in Section 3.4.

3.1 Traffic-Aware Single Camera Tracking (TSCT)

In our MTMCT framework, the first step is SCT, where we implement the TrackletNet Tracker (TNT) [38]. A TNT is a tracklet-based graph clustering approach, where the vertices are generated based on detection association via CNN-based appearance feature and the intersection-over-union (IOU) in the two consecutive frames. While, the edge weights are estimated by a TrackletNet, which is

a Siamese neural network trained to predict the likelihood of the two tracklets belonging to the same object. After the tracklet-based graph is constructed, graph clustering [37] is applied to merge the tracklets of the same vehicle into one single trajectory.

After using TNT to generate the SCT results, we observe that there are some vehicle ID switches due to some *isolated trajectories*, which usually appear while vehicles are waiting for a traffic light. Therefore, we propose TSCT to deal with this issue by generating the traffic-aware zones and performing single camera ReID to reconnect the isolated trajectories caused by the traffic scenarios.

First of all, all the traffic-aware zones within each camera are detected in an unsupervised manner based on the MeanShift clustering algorithm [3] applied on the collected entry/exit measurements. The procedure of traffic-aware zone generation is as follows: 1) use the first and the last positions of all the trajectories from the SCT results as zone nodes; 2) cluster the zones nodes into different groups by apply the MeanShift algorithm.

After the MeanShift, we define a rectangular zone for each group to bound the inside nodes. We denote $N_{e,k}$ as the number of entry nodes and $N_{x,k}$ as the number of exit nodes in the zone k . The traffic-aware density D_{ta} is defined by

$$D_{ta} = 1 - \frac{|N_{e,k} - N_{x,k}|}{N_{e,k} + N_{x,k}}, \quad (1)$$

where D_{ta} needs to be above a threshold ρ_{ta} , the zone will be designated as a traffic-aware zone, as shown in Fig. 2(c).

After the traffic-aware zones are clustered, the next step is to reconnect the isolated trajectories in these zones. Here, we build a queue for each zone to store the ordering and appearance features of the vehicles that are interrupted in the traffic-aware zones. If there is a bounding box of an isolated trajectory that suddenly appears in the traffic-aware zone, we select a trajectory from the queue to compute the appearance similarity. The appearance feature is trained by single camera ReID, which is similar to the cross camera ReID, as explained in Section 3.3.

3.2 Trajectory-based Camera Link Model

Our trajectory-based CLM can be divided into three steps: 1) entry/exit zones generation in each single camera; 2) vehicle trajectory classification according to entry-exit zone pairs in each single camera; 3) camera links and transition time estimation across different cameras. These three steps are described below.

Entry/exit zones generation. With the available routes and the detected entry/exit zones, we can estimate the relationship between each two zones. For a trajectory-based CLM, the procedure of the entry/exit zone generation is similar to the traffic-aware zone generation. The only difference is to calculate the entry and exit density to determine whether the generated zone is an entry/exit zone or not. The entry and exit densities are defined as D_e and D_x , where

$$D_e = \frac{N_{e,k}}{N_{e,k} + N_{x,k}}, \quad D_x = \frac{N_{x,k}}{N_{e,k} + N_{x,k}}. \quad (2)$$

If the density of an entry or exit zone is higher than a threshold ρ_e or ρ_x , this zone will be recognized as an entry or exit zone. There may be multiple entry/exit zones within one camera's FoV.

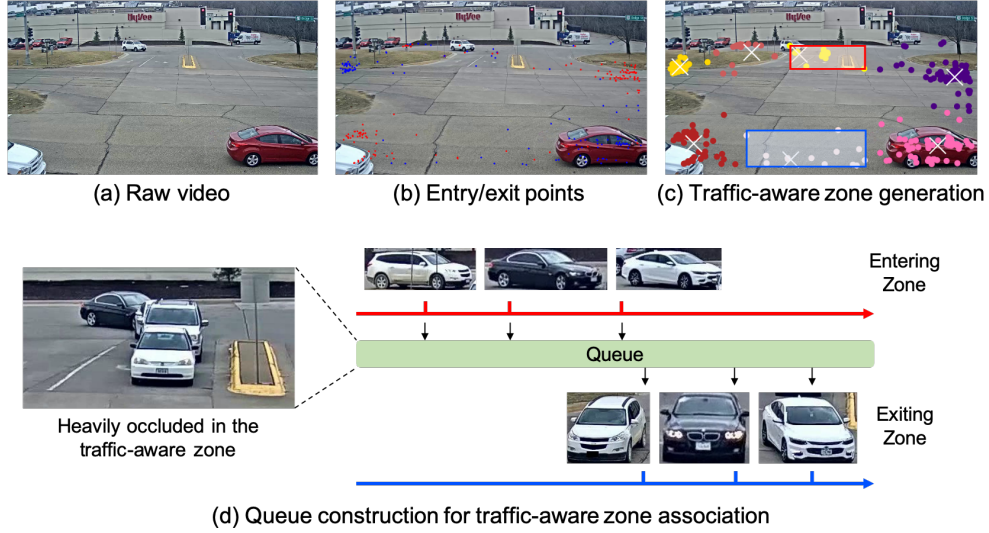


Figure 2: Traffic-aware zone generation. (a) Raw video from a surveillance camera. (b) Start/end points of all trajectories from SCT (red: entry; blue: exit). (c) The clustering result for traffic-aware zone generation from Meanshift (red: stop for traffic light; blue: truncated vehicles). (d) A queue for isolated trajectories is maintained to keep the ordering and appearance features for following single camera ReID.

Vehicle trajectory classification by zone pairs. After the zones are generated, all of the trajectories need to be classified according to entry-exit zone pairs. In our model, an entry-exit zone pair is used to uniquely describe a trajectory, which is called a zone pair trajectory, as shown in Fig. 3(a). In this paper, we generate all possible camera links by using the training data of MTMCT to systematically generate the camera links instead of human labeling. In most cases, the straight and the right-turn trajectories can be described using different zone pairs being passed through. Sometimes the trajectory may not pass through the corresponding zone pair perfectly due to the viewing angle of the camera, i.e., also passes through the neighboring zones associated with the adjacently connected zone pair. In this case, measuring the distance (mismatch) between a tracked vehicle and a zone-pair trajectory is necessary. The distance can be calculated as

$$\text{dist}(P, V) = \sum_{z \in P \cup V} |\mathbb{1}(z \in P) - \alpha_z|, \quad (3)$$

where P denotes the zone-pair trajectory and V is the actual zones gone through by the tracked vehicle, α_z represents the overlapping ratio of the vehicle to zone z , i.e., the overlapping area divided by the vehicle bounding box area. Furthermore, the order of the zones in the zone pair and the tracked vehicle is also considered. Once the order in the tracked vehicle conflicts with the zone pair, the distance between a tracked vehicle and a zone-pair trajectory is set to infinity. Finally, the closest zone-pair trajectory with minimum distance is assigned by comparing the tracked vehicle with all the possible zone-pair trajectories within the camera. An example of distance calculation is shown in Fig. 3(b).

Camera link model construction. Given the locations of the cameras, we can obtain the routing information provided by the training data. The routing information contains all the links between every

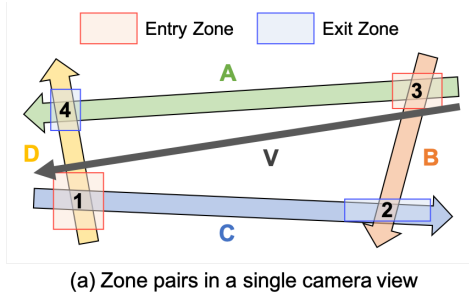
two adjacently connected cameras. If there is one link that connects two cameras without passing through another camera, we define them as a camera link. In other words, if all the routes from the training data between two cameras passed by at least one other camera, this link should not exist in our camera link model.

The camera link and the corresponding transition time of each camera pair can be defined as $\mathcal{T} = (C^s, C^d)$, where $C^s = \{P_i^s\}_{i=1}^m$ is the zone pair trajectories set in the source camera and $C^d = \{P_j^d\}_{j=1}^n$ is that set in the destination camera. Each camera pair can have more than one transition time due to the bi-directional traffic. In the camera pair with the overlapping view, \mathcal{T} usually only contains one single zone pair trajectory, while for the non-overlapping view case, \mathcal{T} can involve multiple zone pair trajectories. An example to explain the concept of our camera link model is shown in Fig. 4(a).

Transition time estimation. To estimate the transition time of each camera link \mathcal{T} , we first define the transition zones z_s and z_d , such that $z_s \in P_i^s$ ($\forall P_i^s \in C^s$) and $z_d \in P_j^d$ ($\forall P_j^d \in C^d$). Then, the transition time can be applied as the temporal constraint for both C^s and C^d . Given a camera link of a tracked vehicle P^s and P^d , i.e., in source camera and destination camera, the transition time is defined as

$$\Delta t = t^s - t^d, \quad (4)$$

where t^s and t^d represent the time of the tracks passing z^s and z^d , respectively. We can then obtain a time window $(\Delta t_{\min}, \Delta t_{\max})$ for each camera link \mathcal{T} so that only the tracked vehicle pairs whose transition time are within the time window are considered as valid. Thus, the search space of the ReID can be greatly reduced by using the appropriate time window. Then, we can use the embedding feature from the ReID model, trajectory-based camera link model, and clustering algorithm to produce the global IDs for MTMCT.



Vehicle Trajectory	Zone	3	2	1	4
	IOU α	0.9	0.1	0.4	0.8

Zone Pair	Distance btw. zone pair and trajectory
A 3→4	$\text{dist}(A, V) = 0.1 + 0.1 + 0.4 + 0.2 = 0.8$
B 3→2	$\text{dist}(B, V) = 0.1 + 0.9 + 0.4 + 0.8 = 2.2$
C 1→2	$\text{dist}(C, V) = \infty$ (wrong order)
D 1→4	$\text{dist}(D, V) = 0.9 + 0.1 + 0.6 + 0.2 = 1.8$

(b) Distances between zone pairs and vehicle trajectory

Figure 3: Illustration of distance calculation between a vehicle trajectory (black) and each entry-exit zone pair. There are four zone pairs (A, B, C, D) with two entry and two exit zones in current frame. The vehicle pass through the four zones with certain IOU in the upper table in (b). The distances are calculated according to Eq. 3. As a result, this vehicle trajectory is classified to zone pair A, which has the smallest distance.

3.3 Cross Camera ReID

After TSCT, the SCT results for each camera are available as the input data for MTMCT. Video-based ReID can achieve better performance than image-based ReID since it can take advantage of temporal continuity of a sequence of image frames instead of a single image. Therefore, an MTMCT system usually uses trajectory-level features for ReID. The feature extractor is based on the ResNet-50 [6], which is pre-trained on ImageNet, and the appearance feature of a vehicle is a 2048-dim vector output by the fully connected layer.

Once the frame-level features are extracted, we use temporal attention (TA) mechanism [4] to aggregate the frame-level features into the clip-level features. After that, we use the average pooling to generate trajectory-level features. In the TA modeling, there are two convolutional networks, one is a spatial convolutional network with 2D convolutions and the other is a temporal convolutional network with 1D convolution. Through training these two networks, an attention vector v_{att} can be obtained to weight the frame-level features f_{frame} , resulting in the clip-level features, where

$$f_{clip} = v_{att} \cdot f_{frame}. \quad (5)$$

In terms of network training, metric learning is adopted to enhance this vehicle ReID task. To train the model in a more efficient way, we adopt the batch sample (BS) scheme [13] in the triplet generation. Overall, in our final loss function, the BS triplet loss

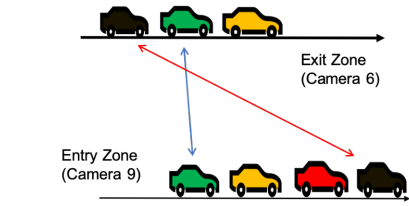
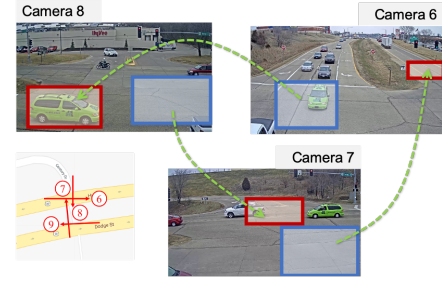


Figure 4: Examples of camera link model and the order constraint. There are three cameras with overlapping FoV, the blue/red bounding boxes represent the exit/entry zones, respectively. According to (a), the location of the exit zone in the Camera 6 is the same as the location of the entry zone of Camera 8, which means the vehicle exits the Camera 6 will immediately appear in the Camera 8. Similarly, Camera 7 connects to Camera 6 and Camera 8 links to Camera 7.

is combined with the cross-entropy loss to jointly exploit distance metric learning and identity classification,

$$\mathcal{L}_{total} = \lambda_1 \mathcal{L}_{BStri} + \lambda_2 \mathcal{L}_{Xent}. \quad (6)$$

The objective of triplet loss is to minimize the feature distance of the same identity and maximize the feature distance of different identity pairs [8]. For the BS triplet loss, the objective is to calculate triplet loss $\mathcal{L}_{BStri}(\theta; \xi)$ in a minibatch defined as

$$\mathcal{L}_{BStri}(\theta; \xi) = \sum_b \sum_{a \in B} l_{triplet}(a), \quad (7)$$

where

$$l_{triplet}(a) = \left[m + \sum_{p \in P(a)} w_p D_{ap} - \sum_{n \in N(a)} w_n D_{an} \right]_+. \quad (8)$$

Here, w_p and w_n are the weightings of positive and negative samples, m represents the margin, D_{ap} and D_{an} are the distances between the anchor sample to the positive sample and negative sample, respectively.

Based on the BS strategy, the weightings of positive and negative samples are defined as follows,

$$w_p = \mathcal{P}(w_p == \text{multinomial}_{x \in P(a)}\{D_{ax}\}), \quad (9)$$

$$w_n = \mathcal{P}(w_n == \text{multinomial}_{x \in N(a)}\{D_{ax}\}),$$

where x_p and x_n are positive and negative samples, respectively.

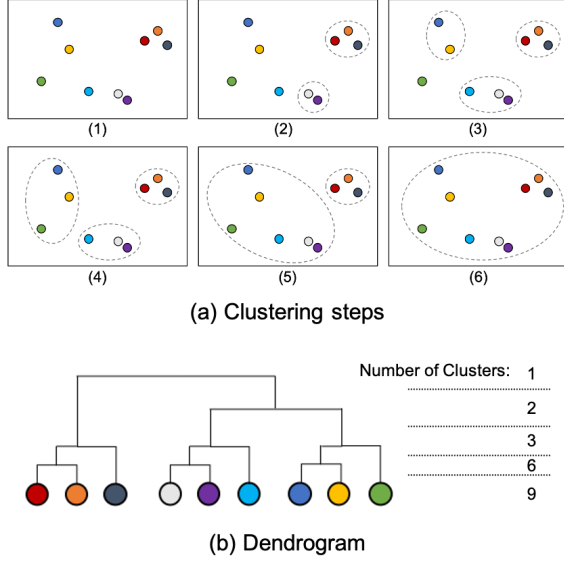


Figure 5: Illustration of hierarchical clustering. An example is shown in (a) for the clustering steps. (b) shows the dendrogram of the example with the number of clusters at different threshold levels.

The cross-entropy (Xent) loss in the training is defined as

$$\mathcal{L}_{Xent} = -\frac{1}{m} \sum_{i=1}^m q(i) \cdot \log(\text{prob}(i)), \quad (10)$$

where $\text{prob}(i)$ is the probability of the probe vehicle belongs to vehicle i , $q(i)$ is the ground truth vector of vehicle i , and m is the number of vehicles in training data.

3.4 Hierarchical Clustering

We perform data association between a pair of single camera trajectories corresponding to an adjacently connected exit/entry zone for multi-camera trajectories utilizing correlation clustering in each separate short time windows. The time window (Δt_{\min} , Δt_{\max}) is generated from CLM. In each window, there is a weighted graph $\mathcal{G} = (\mathcal{V}, \mathcal{E}, \mathcal{W})$, where \mathcal{V} represents the single camera trajectory node set, the weight \mathcal{W} of the edge \mathcal{E} represents the corresponding correlation between the nodes. Therefore, MTMCT can be referred as a correlation clustering problem. Then the issue is to partition the node set into subsets. The single camera trajectories of the same identity should belong to the same subset. Edges in the same subsets accumulate high positive correlations, while edges in the different subsets accumulate high negative correlations. The problem can thus be defined as the following Binary Integer Program (BIP),

$$\begin{aligned} X^* = \arg \max_{\{x_{i,j}\}} & \sum_{(i,j) \in E} w_{i,j} x_{i,j}, \\ \text{s.t. } & x_{i,j} + x_{j,k} \leq 1 + x_{i,k}, \quad \forall i, j, k \in V. \end{aligned} \quad (11)$$

The set X is the set of all possible combinations of assignments to the binary variables $x_{i,j}$. We maximize the summation of $w_{i,j} x_{i,j}$, which rewards edges that connect the same vehicle's multi-camera

Algorithm 1: Hierarchical Clustering

Input : Trajectories set $\Xi = \{\xi_n\}$ from all cameras.
Output : Global ID for all trajectories within all cameras.
Initialize distance matrix M between each two trajectories
 $M \leftarrow \infty$;
for trajectory ξ_i **from** Ξ **do**
 for trajectory ξ_j **from** Ξ **do**
 $M_{i,j} \leftarrow \text{dist}(f(\xi_i), f(\xi_j))$;
 end
end
Flatten and sort the upper triangular part of M in ascending order: $F \leftarrow \text{sort}([M_{i,j}]_{i < j})$;
 $iter \leftarrow 0$, $\delta \leftarrow$ distance threshold;
while $iter < \# \text{ of iterations}$ **do**
 for $m_{i,j}$ **from** F **do**
 if $m_{i,j} < \delta$ **and** valid order constraint for ξ_i, ξ_j **then**
 Assign the same global ID to ξ_i and ξ_j ;
 else
 $m_{i,j} \leftarrow \infty$;
 end
 end
 $iter++$;
end

trajectories and penalizes edges that link to the different vehicles. If the two multi-camera trajectories i, j are from the same vehicle, then $x_{i,j}$ should be assigned 1. The constraints in Eq. 11 enforce the transitivity in the solution.

To reduce the computational complexity, we use hierarchical clustering in our method. Fig. 5 illustrates how to cluster the single camera trajectories into cross camera trajectories. Since the search space of ReID is reduced by the transition time constraint, the Rank-1 accuracy will be close to 1. Therefore, we can greedily select the smallest pair-wise distance to merge the tracked vehicles cross cameras. Furthermore, the order between different tracked vehicles can be used as a constraint to further reduce the search space of the ReID. Due to the traffic scenarios or the road conditions, the orders of vehicles should be almost the same. Take Fig. 4(b) as an example, we will remove the pairs whose orders conflict with those of previously matched pairs. The process will repeat until there is no valid transition pair, or the minimum distance is larger than a threshold.

4 EXPERIMENTS

4.1 Dataset and Evaluation

Our research aims to addressing multi-target multi-camera tracking of vehicles from the video sequences. CityFlow [36] is the largest and the most representative MTMCT dataset for practical scenarios, which is proposed in CVPR 2019 by Nvidia. To the best of our knowledge, it is the only existing city-scale traffic camera dataset. CityFlow contains 3.25 hours of traffic videos collected from 40 cameras across 10 intersections, spanning about 2.5 km, in a mid-sized U.S. city. Moreover, CityFlow covers a diverse set of road traffic types, including intersections, stretches of roadways, and

highways. The length of the training videos is 58.43 minutes, while testing videos are 136.60 minutes in length. There are five scenarios in the CityFlow dataset, three of the scenarios are used for training, and the remaining two are used for testing. In total, the dataset contains 229,680 bounding boxes for 666 distinct annotated vehicle identities with license plates being blackened out. The resolution is at least 960p and the frame rate is 10 FPS. Moreover, the license plates are blocked out in advance due to the privacy issues, i.e., the license plate information is not allowed to be used in the MTMCT.

In terms of implementation details, we use the dataset of the AI City Challenge 2018 [23] for training the TNT in the SCT. Since there are over 3.3K vehicles in the AI City Challenge 2018 dataset, which contains much richer information than the training set in the benchmark dataset. For both feature extraction of single camera ReID and cross camera ReID, we use ResNet-50 as the backbone network, trained with the combination of BS Triplet loss and Xent loss. In TSCT, the dimension of the appearance feature is 512, the time window size is 64, and the batch size is 32. The optimizer used for training TrackletNet is Adam and the learning rate is from 10^{-3} to 10^{-5} for decreasing 10 times in every 2000 steps.

In terms of the single and cross camera ReID, the temporal attention model is trained with tracklet features from ground truth image ReID features. Same as UW IPL [11], we select the 4 as the clip length for each tracklet. The learning rate is 3×10^{-4} , the weight decay is 5×10^{-4} , the batch size is 32, and the network is totally trained for 800 epochs. The similarity estimation of the ReID features is calculated by the Euclidean distance. The input images are resized to 224×224 . We use ResNet-50 pre-trained on ImageNet as the backbone for our model.

For MTMCT, we use IDF1, IDP, and IDR as evaluation metrics. IDF1 [26] is used to rank the performance of each team in the CityFlow dataset. It calculates the ratio of correctly identified detections over the average number of ground truth and computed detections. More specifically, false negative ID (IDFN), true negative ID (IDTN) and true positive ID (IDTP) counts are all used to compute the identification precision (IDP), the identification recall (IDR), and the corresponding F1 score IDF1.

$$\begin{aligned} IDP &= \frac{IDTP}{IDTP + IDFP}, \\ IDR &= \frac{IDTP}{IDTP + IDFN}, \\ IDF1 &= \frac{2IDTP}{2IDTP + IDFP + IDFN}. \end{aligned} \quad (12)$$

The definition of IDFN, IDTN and IDTP are as following,

$$\begin{aligned} IDFN &= \sum_{\tau} \sum_{t \in T_{\tau}} m(\tau, \gamma_m(\tau), t, \Delta), \\ IDFP &= \sum_{\gamma} \sum_{t \in T_{\gamma}} m(\tau_m(\gamma), \gamma, t, \Delta), \\ IDTP &= \sum_{\tau} \text{len}(\tau) - IDFN = \sum_{\gamma} \text{len}(\gamma) - IDFP. \end{aligned} \quad (13)$$

where τ is the ground truth trajectory, $\gamma_m(\tau)$ means the computed trajectory that best matches τ ; γ represents computed trajectory; $\tau_m(\gamma)$ is ground truth trajectory that best matches γ ; t is the frame index; Δ means the IOU threshold that judges whether computed bounding box matches the ground truth bounding box (here we set

Table 1: MTMCT results comparison on CityFlow dataset.

Methods	IDF1
MOANA+BA [36]	0.3950
DeepSORT+BS [36]	0.4140
TC+BA [36]	0.4630
ZeroOne [30]	0.5987
DeepCC [27]	0.5660
LAAM [10]	0.6300
ANU [9]	0.6519
TrafficBrain [7]	0.6653
DDashcam [16]	0.6865
UWIPL[11]	0.7059
Ours	0.7493

$\Delta = 0.5$); $m(\cdot)$ is a mismatch function which is equal to 1 if there is a mismatch at t ; otherwise, $m(\cdot)$ is 0.

4.2 MTMCT Results on CityFlow

In the CityFlow dataset, the spatio-temporal information is useful in improving the performance [7, 11, 16]. Especially, the camera links are applied to achieve the best performance [11]. Moreover, some systems utilize data association graph for MTMCT [9]. Most of the MTMCT methods are based on the tracking-by-detection scheme and adapted for multi-camera views.

The qualitative results are shown in Fig. 6, which shows that our method is generalized well for different cameras and vehicles.

Table 1 compares our methods with the state-of-the-art on the CityFlow benchmark. Moreover, we also compare our method with the state-of-the-art approaches on the DukeMTMC dataset, which is no longer available currently. Locality aware appearance metric (LAAM) [10] is the state-of-the-art approach on DukeMTMC dataset. LAAM improves the performance of DeepCC by training the model based on both intra-camera and inter-camera metrics. The ReID features in DeepCC are extracted by DenseNet-121 with softmax and triplet loss. In terms of LAAM, they use ResNet-50 pre-trained on ImageNet. The tracklet length is set to 10 frames, and the temporal window sizes for SCT and ICT are set to 500 frames and 2400 frames. According to the experimental results, our proposed method outperforms all the state-of-the-art methods, by incorporating the traffic-aware zones for isolated trajectories ReID and also taking advantage of the generated camera link model. Finally, we achieve IDF1 of 74.93% for MTMCT on CityFlow. Moreover, comparing to [11], our system can automatically generate camera links instead of human labeling.

4.3 Ablation Studies

The ablation studies of MTMCT is showed in Table 2, including the combinations of TNT, TSCT, TA, and CLM. The experimental results show that each proposed component helps enhance the robustness. First, we show all modules of the proposed method are necessary. When replacing TSCT with the TNT, IDF1 based on the TA feature drops by 4.3% on MTMCT. A similar but greater accuracy drop can be observed when the TA is replaced by the average pooling. The drop is consistent when using the same tracklet based



Figure 6: Qualitative results of our MTMCT results on CityFlow dataset.

Table 2: The MTMCT performance for different combinations of the proposed method.

TNT	TSCT	TA	CLM	IDF1	IDP	IDR
✓				0.1583	0.4418	0.0959
✓		✓		0.5237	0.6816	0.4221
✓			✓	0.5776	0.5918	0.5779
✓		✓	✓	0.7059	0.6912	0.7211
✓	✓	✓	✓	0.7493	0.8071	0.6918

ReID features. These results show that both the TSCT and TA are necessary components in our system. Second, from the ablation studies, the removal of the CLM causes a greater accuracy drop. The reason is the transition time constraint between cameras improves data association in tracking, so the global matching in ReID is much better in ICT. In the vehicle ReID, high inter-class similarity leads to small appearance variance of the targets. Consequently, after applying the CLM, the MTMCT performance can be largely improved. Then, we show that the TA and CLM are both important, IDF1 can be improved from 15.83% to over 50% by using TA or CLM. Therefore, CLM can improve MTMCT by the general ReID model.

In Table 3, we show the performance of SCT, which favorably compares with the state-of-the-art methods for SCT [34, 37, 40]. DeepSORT [40] is an online method incorporating Kalman-filter-based tracking and the Hungarian algorithm. TC [37] is an offline method using tracklet clustering which is the winner of the AI City Challenge at CVPR 2018 [23]. MOANA [34] is a state-of-the-art approach on the MOTChallenge 2015 3D benchmark. There are three sets of available detection results, i.e., SSD512 [18], YOLOv3 [24] and Faster R-CNN [25], which are provided by the CityFlow dataset. According to [36], SSD512 [18] performs the best and is used by us for comparison. The metrics of SCT include IDF1, Multiple Object

Table 3: MTSC tracking results on CityFlow.

Methods	IDF1	MOTA	MOTP	Recall	MT
DeepSORT [40]	79.5%	68.9%	65.5%	69.2%	756
TC [37]	79.7%	70.3%	65.6%	70.4%	895
MOANA [34]	72.8%	67.0%	65.9%	68.0%	980
Ours	88.4%	79.3%	92.9%	85.1%	1726

Tracking Accuracy (MOTA), Multiple Object Tracking Precision (MOTP), Recall and the mostly tracked targets (MT). According to the experimental results, the proposed TSCT method achieves the best performance.

5 CONCLUSION

In this paper, we propose a novel approach for multi-target multi-camera tracking of vehicles, which includes traffic-aware single camera tracking (TSCT), trajectory-based camera link model (CLM), and vehicle re-identification (ReID). From our experiments, the proposed method is shown to be effective and robust. It also achieves a new state-of-the-art performance on the CityFlow dataset.

ACKNOWLEDGEMENT

This work was partially supported by Electronics and Telecommunications Research Institute (ETRI) grant funded by the Korean government. [20ZD1100, Development of ICT Convergence Technology for Daegu-Gyeongbuk Regional Industry]

REFERENCES

- [1] Herbert Bay, Tinne Tuytelaars, and Luc Van Gool. 2006. Surf: Speeded up robust features. In *European conference on computer vision*. Springer, 404–417.
- [2] Wongun Choi. 2015. Near-online multi-target tracking with aggregated local flow descriptor. In *Proceedings of the IEEE international conference on computer vision*. 3029–3037.

- [3] Dorin Comaniciu and Peter Meer. 2002. Mean shift: A robust approach toward feature space analysis. *IEEE Transactions on pattern analysis and machine intelligence* 24, 5 (2002), 603–619.
- [4] Jiyang Gao and Ram Nevatia. 2018. Revisiting Temporal Modeling for Video-based Person ReID. *arXiv preprint arXiv:1805.02104* (2018).
- [5] Andreas Geiger, Martin Lauer, Christian Wojek, Christoph Stiller, and Raquel Urtasun. 2013. 3d traffic scene understanding from movable platforms. *IEEE transactions on pattern analysis and machine intelligence* 36, 5 (2013), 1012–1025.
- [6] Kaiming He, Xiangyu Zhang, Shaoqing Ren, and Jian Sun. 2016. Deep residual learning for image recognition. In *Proceedings of the IEEE conference on computer vision and pattern recognition*. 770–778.
- [7] Zhiqun He, Yu Lei, Shuai Bai, and Wei Wu. 2019. Multi-Camera vehicle tracking with powerful visual features and spatial-temporal cue. In *Proc. CVPR Workshops*. 203–212.
- [8] Alexander Hermans, Lucas Beyer, and Bastian Leibe. 2017. In defense of the triplet loss for person re-identification. *arXiv preprint arXiv:1703.07737* (2017).
- [9] Yunzhong Hou, Heming Du, and Liang Zheng. 2019. A Locality Aware City-Scale Multi-Camera Vehicle Tracking System. In *Proceedings of the IEEE Conference on Computer Vision and Pattern Recognition Workshops*. 167–174.
- [10] Yunzhong Hou, Liang Zheng, Zhongdao Wang, and Shengjin Wang. 2019. Locality Aware Appearance Metric for Multi-Target Multi-Camera Tracking. *arXiv preprint arXiv:1911.12037* (2019).
- [11] Hung-Min Hsu, Tsung-Wei Huang, Gaoang Wang, Jiarui Cai, Zhichao Lei, and Jenq-Neng Hwang. 2019. Multi-Camera Tracking of Vehicles based on Deep Features Re-ID and Trajectory-Based Camera Link Models. In *AI City Challenge Workshop, IEEE/CVF Computer Vision and Pattern Recognition (CVPR) Conference, Long Beach, California*.
- [12] Tsung-Wei Huang, Jiarui Cai, Hao Yang, Hung-Min Hsu, and Jenq-Neng Hwang. 2019. Multi-View Vehicle Re-Identification using Temporal Attention Model and Metadata Re-ranking. In *AI City Challenge Workshop, IEEE/CVF Computer Vision and Pattern Recognition (CVPR) Conference, Long Beach, California*.
- [13] Ratnesh Kuma, Edwin Weill, Farzin Aghdasi, and Parthasarathy Sriram. 2019. Vehicle re-identification: an efficient baseline using triplet embedding. In *2019 International Joint Conference on Neural Networks (IJCNN)*. IEEE, 1–9.
- [14] Ratnesh Kumar, Guillaume Charpiat, and Monique Thonnat. 2014. Multiple object tracking by efficient graph partitioning. In *Asian Conference on Computer Vision*. Springer, 445–460.
- [15] Young-Gun Lee, Jenq-Neng Hwang, and Zhijun Fang. 2015. Combined estimation of camera link models for human tracking across nonoverlapping cameras. In *2015 IEEE International Conference on Acoustics, Speech and Signal Processing (ICASSP)*. IEEE, 2254–2258.
- [16] Peilun Li, Guozhen Li, Zhangxi Yan, Youzeng Li, Meiqi Lu, Pengfei Xu, Yang Gu, Bing Bai, Yifei Zhang, and DiDi Chuxing. 2019. Spatio-temporal consistency and hierarchical matching for multi-target multi-camera vehicle tracking. In *Proc. CVPR Workshops*. 222–230.
- [17] Hongye Liu, Yonghong Tian, Yaowei Yang, Lu Pang, and Tiejun Huang. 2016. Deep relative distance learning: Tell the difference between similar vehicles. In *Proceedings of the IEEE Conference on Computer Vision and Pattern Recognition*. 2167–2175.
- [18] Wei Liu, Dragomir Anguelov, Dumitru Erhan, Christian Szegedy, Scott Reed, Cheng-Yang Fu, and Alexander C Berg. 2016. Ssd: Single shot multibox detector. In *European conference on computer vision*. Springer, 21–37.
- [19] Xinchun Liu, Wu Liu, Tao Mei, and Huadong Ma. 2016. A deep learning-based approach to progressive vehicle re-identification for urban surveillance. In *European Conference on Computer Vision*. Springer, 869–884.
- [20] Yihang Lou, Yan Bai, Jun Liu, Shiqi Wang, and Lingyu Duan. 2019. Veri-wild: A large dataset and a new method for vehicle re-identification in the wild. In *Proceedings of the IEEE Conference on Computer Vision and Pattern Recognition*. 3235–3243.
- [21] Jonathan Masci, Ueli Meier, Dan Cireşan, and Jürgen Schmidhuber. 2011. Stacked convolutional auto-encoders for hierarchical feature extraction. In *International Conference on Artificial Neural Networks*. Springer, 52–59.
- [22] Anton Milan, Konrad Schindler, and Stefan Roth. 2015. Multi-target tracking by discrete-continuous energy minimization. *IEEE transactions on pattern analysis and machine intelligence* 38, 10 (2015), 2054–2068.
- [23] Milind Naphade, Ming-Ching Chang, Anuj Sharma, David C Anastasiu, Vamsi Jagarlamudi, Pranamesh Chakraborty, Tingting Huang, Shuo Wang, Ming-Yu Liu, Rama Chellappa, et al. 2018. The 2018 nvidia ai city challenge. In *Proceedings of the IEEE Conference on Computer Vision and Pattern Recognition Workshops*. 53–60.
- [24] Joseph Redmon and Ali Farhadi. 2018. Yolov3: An incremental improvement. *arXiv preprint arXiv:1804.02767* (2018).
- [25] Shaoqing Ren, Kaiming He, Ross Girshick, and Jian Sun. 2015. Faster r-cnn: Towards real-time object detection with region proposal networks. In *Advances in neural information processing systems*. 91–99.
- [26] Ergys Ristani, Francesco Solera, Roger Zou, Rita Cucchiara, and Carlo Tomasi. 2016. Performance measures and a data set for multi-target, multi-camera tracking. In *European Conference on Computer Vision*. Springer, 17–35.
- [27] Ergys Ristani and Carlo Tomasi. 2018. Features for Multi-Target Multi-Camera Tracking and Re-Identification. *arXiv preprint arXiv:1803.10859* (2018).
- [28] Ethan Rublee, Vincent Rabaud, Kurt Konolige, and Gary R Bradski. 2011. ORB: An efficient alternative to SIFT or SURF. In *ICCV*, Vol. 11. Citeseer, 2.
- [29] Yantao Shen, Tong Xiao, Hongsheng Li, Shuai Yi, and Xiaogang Wang. 2017. Learning deep neural networks for vehicle re-id with visual-spatio-temporal path proposals. In *Proceedings of the IEEE International Conference on Computer Vision*. 1900–1909.
- [30] Xiao Tan, Zhigang Wang, Minyue Jiang, Xipeng Yang, Jian Wang, Yuan Gao, Xiangbo Su, Xiaoqing Ye, Yuchen Yuan, Dongliang He, et al. 2019. Multi-camera vehicle tracking and re-identification based on visual and spatial-temporal features. In *Proceedings of the IEEE Conference on Computer Vision and Pattern Recognition Workshops*. 275–284.
- [31] Siyu Tang, Bjoern Andres, Miykhaylo Andriluka, and Bernt Schiele. 2015. Sub-graph decomposition for multi-target tracking. In *Proceedings of the IEEE Conference on Computer Vision and Pattern Recognition*. 5033–5041.
- [32] Siyu Tang, Bjoern Andres, Mykhaylo Andriluka, and Bernt Schiele. 2016. Multi-person tracking by multicut and deep matching. In *European Conference on Computer Vision*. Springer, 100–111.
- [33] Siyu Tang, Mykhaylo Andriluka, Bjoern Andres, and Bernt Schiele. 2017. Multiple people tracking by lifted multicut and person reidentification. In *Proceedings of the IEEE Conference on Computer Vision and Pattern Recognition*. 3539–3548.
- [34] Zheng Tang and Jenq-Neng Hwang. 2019. MOANA: An online learned adaptive appearance model for robust multiple object tracking in 3D. *IEEE Access* 7 (2019), 31934–31945.
- [35] Zheng Tang, Milind Naphade, Stan Birchfield, Jonathan Tremblay, William Hodge, Ratnesh Kumar, Shuo Wang, and Xiaodong Yang. 2019. PAMTRI: Pose-Aware Multi-Task Learning for Vehicle Re-Identification Using Highly Randomized Synthetic Data. In *Proceedings of the IEEE International Conference on Computer Vision*. 211–220.
- [36] Zheng Tang, Milind Naphade, Ming-Yu Liu, Xiaodong Yang, Stan Birchfield, Shuo Wang, Ratnesh Kumar, David Anastasiu, and Jenq-Neng Hwang. 2019. Cityflow: A city-scale benchmark for multi-target multi-camera vehicle tracking and re-identification. In *Proceedings of the IEEE Conference on Computer Vision and Pattern Recognition*. 8797–8806.
- [37] Zheng Tang, Gaoang Wang, Hao Xiao, Aotian Zheng, and Jenq-Neng Hwang. 2018. Single-camera and inter-camera vehicle tracking and 3D speed estimation based on fusion of visual and semantic features. In *Proceedings of the IEEE Conference on Computer Vision and Pattern Recognition Workshops*. 108–115.
- [38] Gaoang Wang, Yizhou Wang, Haotian Zhang, Renshu Gu, and Jenq-Neng Hwang. 2019. Exploit the connectivity: Multi-object tracking with trackletnet. In *Proceedings of the 27th ACM International Conference on Multimedia*. 482–490.
- [39] Longyin Wen, Wenbo Li, Junjie Yan, Zhen Lei, Dong Yi, and Stan Z Li. 2014. Multiple target tracking based on undirected hierarchical relation hypergraph. In *Proceedings of the IEEE Conference on Computer Vision and Pattern Recognition*. 1282–1289.
- [40] Nicolai Wojke, Alex Bewley, and Dietrich Paulus. 2017. Simple online and realtime tracking with a deep association metric. In *2017 IEEE international conference on image processing (ICIP)*. IEEE, 3645–3649.
- [41] Xiang Wu, Ran He, Zhenan Sun, and Tieniu Tan. 2018. A light cnn for deep face representation with noisy labels. *IEEE Transactions on Information Forensics and Security* 13, 11 (2018), 2884–2896.
- [42] Hongyi Zhang, Andreas Geiger, and Raquel Urtasun. 2013. Understanding high-level semantics by modeling traffic patterns. In *Proceedings of the IEEE international conference on computer vision*. 3056–3063.
- [43] Xiaofan Zhang, Feng Zhou, Yuanqing Lin, and Shaoting Zhang. 2016. Embedding label structures for fine-grained feature representation. In *Proceedings of the IEEE Conference on Computer Vision and Pattern Recognition*. 1114–1123.
- [44] Zhimeng Zhang, Jianan Wu, Xuan Zhang, and Chi Zhang. 2017. Multi-target, multi-camera tracking by hierarchical clustering: Recent progress on dukemtmc project. *arXiv preprint arXiv:1712.09531* (2017).
- [45] Wenzhi Zhao and Shihong Du. 2016. Spectral-spatial feature extraction for hyperspectral image classification: A dimension reduction and deep learning approach. *IEEE Transactions on Geoscience and Remote Sensing* 54, 8 (2016), 4544–4554.
- [46] Zhun Zhong, Liang Zheng, Donglin Cao, and Shaozi Li. 2017. Re-ranking person re-identification with k-reciprocal encoding. In *Proceedings of the IEEE Conference on Computer Vision and Pattern Recognition*. 1318–1327.
- [47] Yi Zhou and Ling Shao. 2018. Aware attentive multi-view inference for vehicle re-identification. In *Proceedings of the IEEE Conference on Computer Vision and Pattern Recognition*. 6489–6498.